Comparison of Xrn1 and Rat1 5'-3' exoribonucleases in budding yeast supports the unique role of Xrn1 in co-translational mRNA decay

Jose Perez-Ortin[1], A. Jordán-Pla[1], Y. Zhang[2], J. Moreno-García[1], L. Campos-Mata[3], Juana Diez[3], V. Pelechano[2], Jose Garcia-Martinez[1], and Mordechai Choder[4]

[1]Universitat de València
[2]Karolinska Institutet Institutionen for mikrobiologi tumor- och cellbiologi
[3]Universitat Pompeu Fabra
[4]Technion Israel Institute of Technology

July 25, 2023

Abstract

The yeast *Saccharomyces cerevisiae* and most eukaryotes carry two 5'-3' exoribonuclease paralogues that are very similar. In yeast, they are called Xrn1, which shuttles between the nucleus and cytoplasm and executes major cytoplasmic mRNA decay, and Rat1, which carries a strong nuclear localization sequence (NLS) and localizes in the nucleus. Xrn1 is 40% homologous to Rat1 but has an extra ~500 amino acids C-terminal extension. In the cytoplasm, Xrn1 can degrade decapped mRNAs during the last round of translation by ribosomes "co-translational mRNA decay". The division of labor between the two enzymes is still enigmatic and can serve as a paradigm for division of labor of many other paralogues. Here we show that Rat1 is capable of functioning in cytoplasmic mRNA decay, provided that Rat1 remains cytoplasmic due to its NLS disruption (cRat1). This indicates that the actual segregation of the two paralogues plays roles in their specific functions. However, segregation is not sufficient for fully complementing Xrn1 function. Specifically, cRat1 can only partially recover cell volume, mRNA stability, proliferation rate, 5'-3' decay alterations that characterize $\xi\rho\nu1\Delta$ cells. In particular, co-translational decay is only little complemented by cRat1. Adding the Xrn1 C-terminal domain to Rat1 does not improve the phenotypes indicating that lack of C-terminal is not the reason for the partial complementation. Collectively, it seems that during evolution the two paralogues acquire unique features that make the division of work beneficial.

Introduction

In eukaryotes, 5'-3' decay plays a crucial role in controlling RNA processing, quality, and quantity. 5'-3' exoribonucleases (XRNs) are conserved in eukaryotes and play crucial roles in diverse aspects of mRNA and non-coding (nc) RNA processing and degradation. XRNs recognize RNAs with a 5' monophosphate (5'P) end arising from endonucleolytic or exonucleolytic cleavage or decapping, and trim the RNA processively in the 5'-3' direction (Nagarajan et al., 2013; Chang et al., 2011). The molecular functions of XRNs have been mainly studied in the budding yeast *Saccharomyces cerevisiae* , which possesses two XRNs, a mainly cytoplasmic exoribonuclease, Xrn1, and a nuclear exoribonuclease, Xrn2 (also referred to as Rat1) (Amberg et al., 1992; Heyer et al., 1995; Johnson, 1997). In yeast, Xrn1 is responsible for cytoplasmic deadenylation-dependent mRNA 5'-3' exonucleolytic decay (Parker & Song, 2004, Nagarajan et al., 2013). Indeed, the demonstrated activity as 5'-3' exoribonuclease (Larimer & Stevens, 1990, Larimer et al., 1992) is the reason for its Xrn1 (e*x* o*r* ibo*n* uclease*1*) name. Xrn1 5'-3' exonucleolytic activity on mRNAs is fundamental for the decay of both correct and defective molecules, provided that they have a 5'P end caused by either decapping

or endonucleolytic cleavage (Parker & Song, 2004, Nagarajan et al., 2013). Xrn1p can also hydrolyze NAD-capped mRNAs (deNADase activity) and, afterwards, exonucleolytically degrade them processively (4). Its enzymatic activity is highly processive and can even act co-translationally on ribosome-associated mRNAs. In this context, Xrn1 trails the last translating ribosome (Pelechano et al, 2015) with which it physically interacts specifically (Tesina et al., 2019). Xrn1 plays additional roles in mRNA processing and quality control, rRNA processing, tRNA quality and ncRNA decay (Parker & Song, 2004; Nagarajan et al., 2013; Langeberg et al., 2020; Sharma et al., 2022).

Both 5'-3' exoribonucleases are partially homologous (Nagarajan et al., 2013; Kenna et al., 1993) and have been shown to be functionally interchangeable, although they were thought to be restricted to specific cellular compartments: Xrn1 in the cytoplasm and Rat1 in the nucleus (Johnson, 1997). *RAT1* is an essential gene, whereas *XRN1*is not (Johnson, 1997). Ectopic nuclear localization of Xrn1 by the addition of an SV40 nuclear location signal (NLS) can rescue *rat1*lethality, whereas cytoplasmic Rat1, lacking its NLS, can rescue*xrn1 ski2* lethality (Johnson, 1997). *SKI2* encodes a co-factor of the 3'-5' RNA exosome, which is essential for its cytoplasmic function (Johnson & Kolodner, 1995). The enzymatic mechanism of Rat1 is assumed to be processive and similar to that of Xrn1 because it shares the active site and shows extensive conservation around it (Nagarajan et al., 2013; Basu et al., 2021). Rat1 is also a deNADing enzyme similar to Xrn1 (Sharma et al., 2022). Rat1 performs important nuclear activities related to RNA metabolism, including rRNA and snoRNA processing, as well as poly-A^+ dependent and independent mRNA transcription termination (Kim et al., 2004). The existence of both nuclear (Rat1/Xrn2 family) and cytoplasmic (Xrn1 family) 5'-3' exoribonucleases is common in a variety of studied eukaryotes (Chang et al., 2011; Han et al., 2023) and suggests that functional interchangeability extends across species (reviewed in Nagarajan et al., 2013).

Rat1 apparently lacks cytoplasmic functions (Johnson, 1997), whereas it has been shown for Xrn1 that, albeit predominantly cytoplasmic (Johnson, 1997; Haimovich et al., 2013), it also plays important nuclear functions, such as rRNA processing and degradation of defective RNAs (Nagarajan et al., 2013). Xrn1 also acts as a general transcription activator, forming a complex with other decay factors (Haimovich et al., 2013; Medina et al., 2014). The proper cytoplasmic function of Xrn1p requires its shuttling between the cytoplasm and nucleus (Pérez-Ortín & Chavez, 2022), which is made possible by the recently discovered existence of two NLSs (Chattopadhyay et al., 2022). Budding yeast Xrn1 is a very long protein with 1528 amino acids compared to the shorter Rat1 (1006 amino acids). The larger size of Xrn1 is due to an extended C-terminal (Cterm) segment that is absent in Rat1 (Chang et al., 2012), which is a basic domain that is not essential for most *in vivo*functions and is toxic when overexpressed (Page et al., 1998). This feature and the relatively low homology between budding yeast Xrn1 and Rat1 (40% amino acid identity) pose the question of how these two proteins can substitute one another when located in each other's cell compartment (Johnson, 1997).

In this study, our goal was to gain insight into which of the *in vivo* activities of Xrn1 can be substituted with Rat1. We studied two yeast strains that express *RAT1* with defective NLS, the product of which is cytoplasmic (cRat1). We found that cRat1 partially complements many of the natural features of Xrn1, including co-translational mRNA decay. This complementation is not improved by adding Xrn1 Cterm to cRat1 despite the fact that this construction was previously shown to complement other differences in cRat1 activity (Blasco-Moreno et al., 2019). These results support the idea that both 5'-3' exonucleases have functionally redundant activities, but have acquired some unique features, including their cellular localization, that seem to optimize their function and possibly their cooperation. Our results suggest that there are other structural disparities between the two exonucleases, potentially involving distinct binding partners, or the essential import of Xrn1 into the nucleus. These features are crucial for the complete *in vivo* functionality of co-translational mRNA decay..

Materials and Methods

Yeast strains and culture conditions

Yeast cells were grown in YPD (1% yeast extract, 2% peptone, 2% glucose) at 30degC. Pre-cultures were

grown overnight in 250 mL flasks and shaken at 190 rpm. The next day, pre-cultures were diluted to OD_{600} = 0.05 and grown until an OD_{600} of ˜0.5 was reached. Cells were recovered by centrifugation, flash-frozen in liquid nitrogen and stored at -20 oC until needed for Genomic Run-on (GRO) or RNA extraction. Yeast strains were transformed with centromeric plasmids YCpLac33 and pBBM3 following a standard protocol (Gietz & Schiestl, 2007). Yeast strains and plasmids are listed in Supplementary Table S1.

For generation time (GT) estimations, 50 mL of yeast cultures were grown in 250-mL flasks with shaking (190 rpm) at 30degC. Aliquots were taken every 30 min in the exponential phase and their OD_{600}(from 0.05 to 0.7) were measured. The GT (in minutes) in the exponential phase was calculated from growth curves (see Figures 1 and S1).

The median values of cell volumes were calculated by a Coulter-Counter Z series device (Beckman Coulter, USA). The absolute values in femtolitres (fL) and relative values are shown in Figures 1 and S1.

Genomic run-on

Genomic run-on (GRO) was performed as described in (Garcia-Martinez et al., 2004) and as modified in (Oliete-Calvo et al., 2018). Briefly, GRO detects by macroarray hybridization, genome-wide, active elongating RNA polymerase (RNA pol) II, whose density per gene is taken as a measurement of its synthesis rate (SR). At the same time, the protocol allows the mRNA amounts (RA) for all the genes to be measured. mRNA half-lives (HLs) are calculated as RA/SR by assuming steady-state conditions for the transcriptome. The total SR for a given yeast strain was calculated as the sum of individual gene SRs. GRO datasets are available at the Gene Expression Omnibus (GEO) with accession numbers: GSE29519 and GSE198240 (reviewer access code: *mbyjqgschrcfhib*).

mRNA half-life calculations

In order to determine single gene mRNA HLs, transcriptional shut-off was used following the addition of thiolutin up to 5 µg/mL. Samples were collected at 0, 5, 12, 25, 45, 60 and 90 min after thiolutin addition. Samples were analyzed by Northern blot using specific^{32}P-probes as described elsewhere (Pelechano & Pérez-Ortín, 2008).

To determine the global mRNA HL, a dot-blot strategy was followed as described in (García-Martínez et al., 2016). Known amounts of total RNA were spotted onto a nylon membrane and hybridized with a^{32}P-terminal labelled oligo $d(T)_{40}$probe. RNA samples were collected after thiolutin addition at the same times as described for individual mRNAs. The detailed protocol is described in (Benet et al., 2017).

HT-5Pseq and 5'-Capseq protocols

HT-5Pseq libraries were prepared as previously reported (Zhang & Pelechano, 2021). Briefly, 6 µg of DNA-free total RNA were directly ligated with the RNA/RNA oligo containing UMI (RNA rP5_RND oligo). Ligated RNA was reverse-transcribed and primed with Illumina PE2 compatible oligos containing random hexamers and oligo-dT. RNA in RNA/DNA hybrid was depleted by sodium hydroxide with 20-minute incubation at 65°C. Ribosomal RNAs were depleted using DSN (duplex-specific nuclease) with the mixture of ribosomal DNA probes. Samples were amplified by PCR and sequenced in an Illumina NextSeq 500 instrument using 60 sequencing cycles for read1 and 15 cycles for read 2.

For 5'Capseq, 5'capped mRNAs were captured as previously described (Pelechano et al., 2016). Specifically, 10 µg total RNA were treated with calf intestinal alkaline phosphatase (NEB, CIP) to remove 5'P molecules (fragmented and non-capped). After purification, mRNA 5'caps were removed by Cap-Clip (Biozyme), which resulted in 5'P molecules from previously capped molecules. The following steps were the same as that described for HT-5Pseq (see above) with variations only for skipping removing ribosomal RNA. Datasets are available from GEO database: GSE119114 for the 5Cap-seq data, GSE193992 (reviewer access code:*ahadwoocjrivtot*) for HT-5Pseq data.

Protein expression levels measurement by Western blotting

To check for protein expression levels, yeast cells were transformed with the corresponding plasmids and grown as specified in a previous section. Two optical density (OD) units were harvested by centrifugation. Total proteins were extracted from the equivalent number of cells and loaded on sodium dodecyl sulfate polyacrylamide gel electrophoresis (SDS-PAGE) to be separated according to their molecular weight. Next samples were immunoblotted on a nitrocellulose membrane for 90 min at 100 V on ice, as previously described (Ishikawa et al., 1997). Antibodies against FLAG (Sigma-Aldrich), PGK (Invitrogen) and Xrn1 (a gift from A. Johnson) were used. Detection of proteins was performed with an Amersham Imager 600.

Bioinformatics procedures

HT-5Pseq reads were trimmed with a 3'-sequencing adapter using cutadapt V1.16 (http://gensoft.pasteur.fr/docs/cutadapt/1.6/index.html). The 8-nt random barcodes on the 5 ends of the reads were extracted and added to the header of the fastq file as the UMI employing UMI-tools. 5'P reads were mapped to *S. cerevisiae* (SGD R64-1-1) using STAR 2.7.0 with parameter –alignEndsType Extend5pOfRead1 to exclude soft-clipped bases on the 5 end. After removing PCR duplications using UMI-tools, analysis of the 5 ends positions was performed using the Fivepseq package (Nersisyan et al., 2020, http://pelechanolab.com/software/fivepseq), including the relative distance to start and stop codons. In particular, the unique 5´ mRNA reads within biological samples were summed and subsequently normalized to reads per million (rpm). Standalone normalized average density plots around genomic features were calculated with R and Python software ngs.plot v2.61 (Schen et al., 2014) using indexed alignment files as inputs and the internal SacCer3 database annotation as reference. The statistical robustness parameter, which filters out 0.5% of the genes with the most extreme (high and low) count values, was applied to all calculations.

5'Cap reads were processed as described for HT-5Pseq reads. In general, 5'Cap reads were trimmed using a 3'-sequencing adapter and the extracted 8-nt random barcodes were used as UMI. The 5'Cap reads were mapped to*S. cerevisiae* (SGD R64-1-1) using STAR 2.7.0. PCR duplicates were removed using means of UMI-tools.

Heatmaps and the accompanying average metaplots displaying HT-5Pseq alongside the 5'Capseq datasets were generated using the bamCoverage, computeMatrix and plotHeatmap functions from the deepTools2 package (Ramírez et al., 2026). The transcription start site (TSS) and polyA site (pA) annotations were taken from (Xu et al., 2009). Spearman correlation values and statistical test result asterisks were inserted into ggplot2-generated plots using the ggpubr package (*https://rpkgs.datanovia.com/ggpubr*).

Results

Cytoplasmic Rat1 partially replaces Xrn1 in global phenotypes

Rat1 derivative lacking the NLS (cRat1) which mis-localizes to the cytoplasm, was complements some of the cytoplasmic functions of Xrn1, including the defective growth phenotype of the *xrn1[?]* strain (Johnson, 1997; Blasco-Moreno et al., 2019), growth in the presence of benomyl (Johnson, 1997) and the stability of some viral mRNAs (Blasco-Moreno et al., 2019). In the present study, we investigated whether cRat1 complemented the global physiological phenotypes of the*xrn1[?]* strain, including the cell volume, proliferation rate and mRNA stabilities. We transformed the wild-type and *xrn1[?]* strains with a centromeric plasmid containing the cRat1 gene (pBBM3) using an empty vector (YCpLac33) as a control. Notably, the wild-type strain expressing cRat1 also expressed the endogenous wild-type (including NLS) nuclear Rat1 version (Blasco-Moreno et al., 2019). In this study, these yeast strains are referred to as cRat1 and wt+cRat1 for simplification (Supplementary Table S1). Using this series of four strains we analyzed global poly(A) mRNA stability by transcription shutoff with thiolutin and dot-blot hybridization of time-course samples. We found that cRat1 reverses most of the global increase in mRNA stability caused by Xrn1 depletion (1.38x *vs.* 2.43x, regarding the wild-type considered as 1x; Figure 1A). On the other hand, the addition of cRat1 to a wild-type strain with natural Xrn1 in the cytoplasm did not alter poly(A) decay (0.98x), which suggests a minor role of cRat1 in mRNA decay when endogenous Xrn1 is also present. Finally, cRat1 partially restored the generation time and cell size of the wild-type (Figure 1A).

To verify cRat1 expression, we constructed and analyzed a series of four strains in which the cRat1 protein has a 3xFLAG epitope in its C-terminal part, and validated its expression by western blotting in yeast cells (Figure S1A). The 3xFLAG epitope was necessary to observe the cRat1 expression because 1xFLAG version does not allow detection (Supplementary Figure S1A) but partially affects the strain proliferation rate (Figure S1D). cRat1 without the FLAG epitope, but expressed from the same construct (see Supplementary Table S1) grew similarly to the wild-type (Figure S1D). In these strains we measured mRNA half-lives in two individual mRNAs with medium (*RPL25*) and high (*ACT1*) mRNA stability in an *xrn1[?]* strain, and found that cRat1-3xFLAG restored wild-type stabilities (Figure S1B). To further assess the effect of cRat1 on mRNA stability, we analyzed global poly(A) decay. This analysis showed that cRat1-3xFLAG partially restored wild-type global poly(A) mRNA stabilities (Figure S1C) similar to the cRat1 version (Figure 1A). The generation time and cell size were closer to those of the wild type but not fully recovered (Figures S1C and S1D). as in the case of the strains without the FLAG epitope (Figure 1A). Interestingly, the non-cytoplasmic version of Rat1 with FLAG epitopes did not rescue the growth defect of the *xrn1[?]* strain (Supplementary Figure S1D). We conclude that cRat1 with or without the FLAG epitope behaves similarly in the phenotypes analyzed, although the FLAG epitope has a certain detrimental effect. The actual cell volumes, mRNA global stabilities and generation times for both sets of four strains (Figures 1 and S1) are not quantitatively identical but they qualitatively confirm that cRat1 partially restores global phenotypes in an *xrn1[?]* background.

As cells lacking Xrn1 displayed a strong global down-regulation of RNA pol II-based transcriptional activity (Haimovich et al., 2013), we next examined whether cRat1 would mitigate the effects on global RNA pol II synthesis rates. By means of Genomic run-on (GRO), we found that mRNA synthesis rate in $\xi\rho\nu1\Delta$ was 0.36x that of wild type, whereas addition of cRat1 partially compensated this drop (0.63xFigure 1B). This partial compensation suggests that the decrease in RNA pol II synthesis rates in the *xrn1[?]* mutants was due not only to the absence of Xrn1 as a transcription activator (Medina et al, 2014), but also to the indirect effect of its lower growth rate on synthesis rates (García-Martínez et al., 2016). Alternatively, or in addition, it is possible that 5'-3' mRNA decay *per se* is important for transcription. Interestingly, the global synthesis rates of cRat1 added to a wild-type strain slightly, but significantly, increased (1.15x; Figure 1B) without having a noticeable effect on global mRNA stabilities (Figure 1A).

The compensation in mRNA synthesis rates and stabilities in a cRat1 strain showed a strong bias in individual mRNA synthesis rates and stabilities: the more affected mRNAs in either one in *xrn1[?]* were more compensated after cRat1 addition (Supplementary Figure S2). However, the analysis of the transcriptome-wide differential expression in *xrn1[?]* and the wild-type strains supplemented with cRat1 did not show strong biases in either synthesis rates or mRNA stabilities towards specific gene categories (Supplementary Table S2). This indicates that cRat1 does not have a significant bias in the mRNAs of genes belonging to functional groups, but is mostly related to the actual synthesis and decay rates of mRNAs.

Cytoplasmic Rat1 can function co-translationally in mRNA 5'-3' exonuclease, albeit inefficiently

A quintessential function of Xrn1 is to degrade decapped mRNA during its last round of translation. This helps terminating translation and contributes to half-lives of many mRNAs (see Introduction). We next investigated whether cRat1 could perform ribosome-associated co-translational decay. For this end, we measured the presence of 5'-Phosphate-containing mRNAs genome wide by 5'P degradome RNA sequencing (HT-5Pseq) on both sets of four strains: a) the set of strains transformed with a plasmid containing the Rat1-[?]NLS version (cRat1) without FLAG epitopes or with the empty vector (Figure 2); and b) the set of strains (wild-type and *xrn1[?]*) transformed, or not, with cRat1-3xFLAG (Supplementary Figure S3). We decided to use the FLAG tagged cRat1 as we could be sure about its equal level in all the studied strains (Fig. S3), whereas using the untagged strain was made to make sure that Rat1 function was not compromised.

The wild-type HT-5Pseq metagene profile was characterized by a 3-nucleotide periodicity pattern and a prominent peak of HT-5Pseq reads at -17 nt from the STOP codon (Pelechano et al, 2015). HT-5Pseq

measures the distance between the 5'-3'exonuclease and trailing ribosome during co-translational mRNA decay. We have previously shown that the distance between the 5'P of the mRNA undergoing degradation and the first base of the termination codon is 17 nt at the A site of the trailing ribosome (Pelechano et al, 2015; Zhang & Pelechano, 2021). This distance reflects the steric protection offered by the ribosome to the *in vivo* trimming action of Xrn1p. In contrast to wild-type the -17 nt peak was completely lost in *xrn1[?]* and, in the 5'UTR, reads accumulated in the zone immediately upstream of the AUG codon (Figure 2A). cRat1 partially restored the wild-type metagene profile to show intermediate levels for the 5'-upstream and -17 nt peaks (Fig. 2 left and right panels, respectively). An approach to evaluate genuine ribosome occupancy was to determine how well the coding frame was protected from 5' to 3' decay in relation to the other two frames. The ratio between the protected frame and the other frames was designated as the "frame protection index" (FPI) (Pelechano et al, 2015). This index measures the effectiveness of single-nucleotide coupling between nuclease activity and ribosome position. As expected, the FPI was compromised in*xrn1[?]* cells (Figure 2B). The expression of cRat1 in the*ξρν1Δ* cells only partially recovered the FPI (from 0.79 in*ξρν1Δ* increased to 0.82 in cRat1, compared to value 1 for the wild-type FPI; see Figure 2B). This finding suggests that Rat1 is inefficient, closely following the ribosome position during co-translational mRNA decay when placed in the cytoplasm. This might reflect either differences in the enzyme localization, configuration or processivity.

Given that HT-5Pseq reads accumulate at the 3' (close to the STOP codon) in wild-type cells and shifted to 5' (close to the AUG codon) in*xrn1[?]* , we reasoned that the proportion of reads in these two regions could serve as a proxy for the processivity of the 5'-3' decay level once decay has started, taken as either a genome-wide average or a per-gene index. To calculate this 3' *vs.* 5' proportion for the wild-type, *xrn1[?]* and cRat1 strains, we first made metagene profiles by spanning the entire gene body (Figure 2C), and then compared the number of reads in the last 20% *vs* . the first 20% of the average gene body region. These 3'/5' indices showed that expressing cRat1 in *xrn1[?]* was half as efficient as the wild-type in 5'-3' decay (Figure 2D). We next used the per-gene 3'/5' indices to investigate whether sets of functionally related genes were skewed towards any end of the range. A functional classification analysis of the wild-type revealed that the 250 genes with the highest values in the 3'/5' index (high 5'-3' degradation: Figure, 2E upper panel) were enriched in Gene Ontology (GO, Biological Process) terms related to cell cycle and stress response (not shown), whereas the 250 genes with the lowest values (low 5'-3' degradation: Figure 2E, lower panel) were enriched in GOs related to mitochondria and glucose metabolism, although with low significance (not shown). Next, we generated metagene plots for specific gene sets and observed that while the overall shapes of profiles slightly differed for the various groups, the proportions of reads between samples remained approximately the same in all four yeast strains (Supplementary Figure S3B). This result indicates that the lack of Xrn1 (*xrn1[?]*) and its substitution by cRat1 have transcriptome-wide effects. The heatmaps of the individual genes ordered by 5'UTR length (Figure 2F and Supplementary Figure S4) show that the average metagene plots (Figure 2A/C) represent truly uniform behavior for most yeast mRNAs, with two stronger regions at the 5': being most reads associated with the TSS (see Supplementary Figure S4) and ordered according to 5'UTR length, and a minor one located around the AUG codon as we have previously described for multiple species (Huch et al., 2023). This distribution is clearly observed in the summary average count metagene plots (top panels in Figures 2F and S4). The TSS peak detected by HT-5Pseq was particularly clear for *xrn1[?],* and slightly less so for cRat1. The position of this peak corresponded to the canonical capped TSS full-length molecules (as measured by 5CapSeq, the rightmost lane in Figures 2F and S4). Altogether, these results suggest that in *xrn1[?]* , and to a lesser extent in cRat1, a large fraction of the 5'P-detected molecules corresponds to decapped full-length mRNAs.

FPI reflects single-nucleotide coupling between co-translational decay and the ribosome position along the coding region, while the 3'/5' ratio reflects the processivity of the 5'-3' exonuclease activity and ribosome protection along mRNA. The 3'/5' index is mainly influenced by translation initiation and termination, which are the two regions where ribosomes tend to pause the most. Because in the wild-type pausing at the stop codon lasts longer than pausing at the start codon, the general 3'/5' ratio is expected to be higher than 1. A slow 5'-3' decay results in a 3'/5' index lower than 1 (negative Log_2 ratio in Figure 2D). Nevertheless, the translation machinery can also protect mRNA from 5'-3' decay, perhaps because the cap is protected

(e.g., by eIF4F). Indeed, highly translated mRNAs are less prone to global co-translational decay (Pelechano et al, 2015) and 5'-3' decay. In fact, the 3'/5' index shows a statistically significant inverse correlation with mRNA stability and individual translation rate in wild-type cells (TLRi data from Forés-Martos et al., 2021) (Figure 2G and Supplemental Figure S5). These correlations support the notion that the higher the ribosome density (related to TLRi), the greater the protection against 5'-3' decay, and the higher the mRNA stability. This effect depends on Xrn1 because the negative correlation disappears in *xrn1[?]* , which is consistent with Xrn1 being the major 5'-3' exonuclease (Haimovich et al., 2013; Parker, 2012). The substitution of Xrn1 for cRat1, however, cannot restore ribosome density dependence (Figure S5), consistent with the poor capacity of Rat1 to complement the function of Xrn1 in co-translational decay.

The C-terminus of Xrn1 does not complement the defect in co-translational decay that characterizes the cRat1 function

The inability of cRat1 to fully complement *ξρν1Δ* phenotypes, including the turnover of cytoplasmic mRNAs, suggests that cRat1 does not recognize the uncapped mRNAs, unlike Xrn1 does, or it is not localized close enough to the 5' ends of cytoplasmic mRNAs. In a previous study, we demonstrated that cRat1 was unable to properly regulate the translation of a subset of membrane protein-coding mRNAs because it lacked the C-terminal domain of Xrn1 (Blasco-Moreno et al., 2019). Therefore, we reasoned that the large unstructured domain of Xrn1, which seems to be necessary for interaction with the 5'UTR of these specific mRNAs, might also be necessary to achieve wild-type global 5'-3' exonuclease activity and co-translational 5'-decay levels.

Therefore, to investigate the possible function of Xrn1 Cterm, we used it to create a fusion protein, cRat1-Cterm-3xFLAG, and expressed it in an *ξρν1Δ* background. The protein levels were somewhat lower than those of regular cRat1-3xFLAG, probably because of the much larger fusion protein size (Supplementary Figure S6A). It is important to note that cRat1-Cterm with a FLAG epitope had no noticeable effect on the 5'-3' exonuclease activity of cRat1 (see Figures 2 and S3). Both the cell growth and co-translational decay defects of *xrn1[?]* were compensated only partially by cRat1-Cterm to a similar extent as by regular cRat1 (see the cRat1-Cterm profiles in Figures 2A, C), suggesting that Xrn1 performs specific functions that cannot be replaced with Rat1, even when their main structural difference is minimized using a Rat1-Xrn1-Cterm chimera.

Discussion

During evolution, organisms have accumulated paralogues. As this is a widespread phenomenon, a question was raised regarding the functions of paralogues, do they serve as backups, or each paralogue has acquired a unique function? Here we focus on two paralogues, Rat1 functions mainly, if not exclusively, in the nucleus, whereas Xrn1 shuttles between the nucleus and cytoplasm and accumulates in the cytoplasm. As these paralogues are active in different compartments, the issue of their potential capacity is especially interesting. It was proposed that the two paralogues are fully replaceable, and their distinct functions are attributed to their cellular localization (Johnson, 1997). Xrn1 is a highly conserved and exceptionally large protein (175 kDa in yeast) with multiple biological functions in many eukaryotes. Many of these functions can be attributed to its enzymatic 5'-3' exonuclease activity which acts on several types of RNAs. Rat1 is smaller (116 kDa in yeast) and also functions in several nuclear RNAs decay pathways, including those linked to RNA pol II-coupled mRNA transcriptional termination (Kim et al., 2004). Both Xrn1 and Rat1 substrates are single-stranded unstructured 5'Phosphate end with lengths of at least four nucleotides (Nagarajan et al., 2013; Basu et al., 2021). Many of Xrn1 functions require only two-thirds of the molecule, which is homologous to Rat1. The last Xrn1 C-terminal third (CTD) is apparently unstructured, less conserved, and not important for some functions (Bashkirov et al., 1995). CTD is necessary for Xrn1 interaction with eIF4G to regulate the translation of certain membrane-protein-encoding mRNAs (Blasco-Moreno et al., 2019). It also serves as an interaction platform for other proteins in higher eukaryotes (Braun et al., 2012). Being unstructured, it is likely involved in Xrn1 capacity to reside in liquid-liquid phase-separated droplets (Currie et al., 2020). To perform nuclear functions, Xrn1 shuttles between the cytoplasm and nucleus (Haimovich et al., 2013; Medina et al., 2014; Pérez-Ortín & Chavez, 2022). Nuclear import depends on two NLSs whereas export to the cytoplasm is proposed to be mediated by its ability to bind or "imprint" mRNAs (Chattopadhyay

et al., 2022). Shuttling and mRNA imprinting have been shown to affect both mRNAs synthesis and decay (Chattopadhyay et al., 2022). Thus, although these two paralogues are very similar and both have highly conserved domains that carry 5'-3' exonuclease activity, their cellular localization is different. This raised the question whether this difference in localization is the main reason for their disparate functions. This question was previously addressed by A. Johnson (1997), who conclusdedthat they are functionally interchangeable. Because we have gained more information about these paralogues since 1997, we decided to reevaluate this conclusion. The above question is important for understanding the functions of these two paralogues. Moreover, addressing this issue can also serve as a paradigm for other paralogues with identical enzymatic activity.

To this end, we investigated whether the cytoplasmic function of Xrn1 could be performed by its nuclear counterpart Rat1. We found that a cytoplasmic version of Rat1 (cRat1) can only partially complement the 5'-3' exonuclease activity of the missing Xrn1 in the cytoplasm. Even fusing the Xrn1 CTD to the C-terminus of cRat1 (cRat1-Cterm), did not improve cRat1 performance. Specifically, although cRat1 could mostly recover cell volume, growth rate and global mRNA decay, it fails to fully recover co-translational mRNA decay. Previously, we found that deletion of XRN1 resulted in defective transcription, which was attributed to both direct and indirect effects (Haimovich et al., 2013; Medina et al., 2014; Chattopadhyay et al., 2022). Direct effects should be the result of the loss of the direct function of Xrn1 in transcription activation (Xrn1 is a component of the pre-initiation complex), whereas indirect effects are probably the consequence of slow growth of the strain. Given the observation that Rat1 recovers the growth defect of xrn1? cell, the cRat1-mediated increase in transcription of these $\xi\rho\nu1\Delta$ cells might be due to the growth rate effect. Interestingly, cRat1 could slightly, but significantly, increase transcription in wild-type cells. cRat1 might compete with Xrn1 on binding the substrates. This possible competition could provide a plausible explanation for this transcriptional increase in wild-type cells, as cRat1 could increase the amount of free Xrn1, capable of importing to the nucleus and activating transcription. In addition, it is possible that mRNA decay *per se* enhances transcription (e.g., by supplying more nucleotides).

In the absence of *XRN1* , cRat1 can provide some mRNA buffering activity (Figure 1A). Hence, it seems that a partial mRNA buffering can be accomplished without Xrn1 and without its specific shuttling feature. Interestingly, we found that compensation introduced by cRat1 is proportional to the defect caused by the absence of Xrn1 (Figure S2). Maybe, the observation that decapping rate is one of the limiting activities in mRNA decay (Parker 2012) is relevant for this correlation. We propose that mRNA degradation *per se* can provide some buffering, probably together with other pathways and partners that act in concert or in parallel. In particular, our results suggest that the transcription activation capacity of Xrn1 is not absolutely required for buffering (assuming that Rat1 does not have this function) However, since this buffering is partial, it is clear that mRNA decay is not sufficient to provide full buffering. Maybe the transcription activation and the specific shuttling features of Xrn1 are required for efficient buffering.

The effect of cRat1 expression on the start of 5'-3' mRNA decay after decapping (HT-5Pseq profiles and the 3'/5' index) of $\xi\rho\nu1\Delta$ cells is partial. Using heatmaps of the HT-5Pseq data, we noticed that in wild-type cells, the peak at the TSS was clearly less strong than in the$\xi\rho\nu1\Delta$ cells (Figures 2F and S4), which suggests that Xrn1 is located in the vicinity of the RNA 5' end, and is ready to act as soon as the cap is removed. cRat1 did not significantly improve the$\xi\rho\nu1\Delta$ pattern. The 3 nt degradation pattern inside the ORFs in a$\xi\nu\rho1\Delta$ is lost. Taking the relative FPI value of this mutant lacking any cytoplasmic 5'-3' exoribonuclease as a bottom reference (0.79) and the wild-type value as 1, the cRat1 strain only increases the FPI value by 14% (up to 0.82) indicating that cRat1 is not a good substitute for Xrn1 closely following the ribosome position during co-translational mRNA decay. Given that Cterm of Xrn1 does not improve the function of cRat1 we conclude that the N-terminal two-thirds of Xrn1 contain all the determinants needed for 5'-3'co-translational decay. This idea is supported by the fact that the Xrn1 interacts with ribosomes via the 1-772 amino acids region and no interaction is detected with its Cterm domain (Tesina et al., 2019). The reason why cRat1 can hardly replace Xrn1 in co-translational decay remains to be determined. It is possible that the imprinting capacity of Xrn1 (Chattopadhyay et al., 2022) plays some role. The association of the imprinted Xrn1 with mRNA also in the cytoplasm may localize Xrn1 near the 5' end of the mRNA, and upon decapping it is

available immediately for degradation. We note that the expression level of cRat1 is probably lower than the cytoplasmic level of Xrn1 in the wild type. However, given that it has been shown that the cytoplasmic level of Xrn1 is not limiting for 5'-3' mRNA decay (Chattopadhyay et al., 2022) we consider that this is not the reason of the differences found between cRat1 and wild type cells.

XRN1 and *RAT1* are paralogous genes that are not derived from the whole-genome duplication (Wolfe, 2015) but from an older small-scale duplication (Fares et al., 2013). They show intermediate homology divergence and are present in most eukaryotes from yeast to humans (Parker & Song, 2004), suggesting a long time for sequence divergence. However, they can reciprocally rescue each other's lethal phenotypes in yeast (Johnson, 1997). Here we confirm that their exonuclease activities are interchangeable. Nevertheless, it seems that the specialization of the two 5'-3' exonucleases makes them different in terms of the interactive partners they bind to, perhaps affected by the presence or absence of Xrn1 Cterm. However, the addition of Xrn1-Cterm to Rat1 was insufficient to make it fully interchangeable with Xrn1. Therefore, it is important to note that, their subcellular distribution and dynamics are critical for their differential activities. Rat1 is predominantly nuclear whereas Xrn1 is largely cytoplasmic (Sharma et al., 2022; Johnson, 1997; Haimovich et al., 2013). Rat1 can substitute for Xrn1 when its NLS is deleted and becomes cytoplasmic (Sharma et al., 2022, this paper) whereas Xrn1 can only complement the *rat1*mutant when it overexpressed from a multicopy plasmid and is fused to a strong SV40 large-T-antigen NLS (Johnson, 1997). Xrn1, moreover, has the capacity to shuttle. Thus, the number of nuclear and cytoplasmic 5'-3' exonuclease molecules and the capacity to shuttle determine the functional difference between these two exonucleases. These features should have appeared early during eukaryotic evolution and made it impossible to completely substitute one protein for the other, despite their similar and partially interchangeable exonuclease activities.

Funding

This work was funded with grants from: the Spanish MCIN/AEI/10.13039/501100011033 [PID2020-112853GB-C31] to J.E.P-O; the Swedish Foundation's Starting Grant (Ragnar Söderberg Foundation); the Swedish Research Council [VR 2020-01480, 2021-06112 and 2019-02335]; a Wallenberg Academy Fellowship [2021.0167]; Vinnova (2020-03620), Karolinska Institutet (SciLifeLab Fellowship, SFO and KI funds) to V.P. and the Israel Science Foundation (ISF) for M.C., Y.Z. is funded by a fellowship from the China Scholarship Council. The computational analysis was partially performed on the resources provided by the Swedish National Infrastructure for Computing (SNIC) through the Uppsala Multidisciplinary Center for Advanced Computational Science (UPPMAX), partially funded by the Swedish Research Council with grant agreement no. 2018-05973.

Author Contributions

A. Jordán-Pla: validation, formal analysis. Y. Zhang: Investigation. Formal analysis; J. Moreno-García: Investigation; L. de Campos-Mata: Investigation; M. Choder: Conceptualization, Manuscript writing; J. Díez: Conceptualization; V. Pelechano: Conceptualization, Funding; J. García-Martínez: Investigation, Formal analysis; J.E. Pérez-Ortín: Study design, Investigation, Formal analysis, Manuscript writing, Funding.

Acknowledgements

We acknowledge A. Johnson for the gift of the Xrn1 antibody.

Conflict of interest

The authors declare no conflict of interest

Figure legends

Figure 1.- The cytoplasmic version of the Rat1 protein (cRat1) restores mostly, but not totally, the main phenotypes of a *xrn1[?]*strain. A) Generation times (GT), cell volumes and global poly(A) mRNA stability were determined as described in the Materials and Methods section for the four strains. Values were relativized to those of the wild-type (wt) strain (transformed with the empty plasmid YCpLac33), which was taken as 1.00. As a result, the wild-type (wt) values lack standard deviation (SD). The experiments

were repeated three times and averaged. The actual values for wt were 80+-9 min for GT, 65+-2 fL for cell volume and 59+-6 min for poly(A) mRNA stability. B) The synthesis rates (SR) for all RNA pol II genes (in arbitrary units, a.u.) were calculated by GRO, as described in the Materials and Methods. The distribution of all values and their medians are shown in the box and whiskers representation. All comparisons are significant at the < 0.001 level (***).

Figure 2.- The cytoplasmic version of Rat1 protein (cRat1) partially restores the wild-type HT-5Pseq profile in a *xrn[?]1*strain. The C–terminal region of Xrn1 does not improve the performance of cRat1 . A) HT-5Pseq high-resolution plots showing the profiles of wild-type (wt) and *xrn1[?]* strains transformed with the empty YCpLac33 plasmid or its version (pBBM3), including the truncated cytoplasmic version of Rat1 (cRat1) without the nuclear localization sequence (NLS) or the same construct fused to the C-terminal domain of Xrn1 (cRat1-Cterm). The metagene analysis for 5'P read coverage in relation to the open reading frame (ORF) start (left) and stop codons (right) are shown in the samples described above. Three biological replicates of each experiment were merged for each sample. B) Relative frame protection index (FPI) of the four strains analyzed in A). The median FPI for the wt was taken as 1. *** = $P < 0.001$; **** = $P < 0.0001$. C) Average metagene plots of normalized HT-5Pseq read counts around the protein-coding genes. Gene body read coverage is represented as a percentage of the total length of the ORF, whereas the flanking regions around the START and STOP codons represent the real distances from the reference points (represented as base pair length). Shadowed vertical areas highlight the 20% length of both transcribed region ends used for the calculation of the 3'/5' index. D) Violin plot of $\log_2$ 3'/5' index values for the wt, xrn1Δ and cRat1 strains. E) Average metagene plots of 250 genes with the highest 3'/5' index values (top panel) or 250 genes with the lowest (bottom panel) in wt. F) Heatmaps of HT-5Pseq and 5'Capseq data for all the individual protein-coding genes aligned by their START codon and ordered, from top to bottom, by increasing the 5'UTR length. The corresponding summary average count metagene plots are shown at the top of each heatmap. G) Violin plots of the $\log_2$ frame protection index (FPI) (left) or 3'/5' index (right) values in wt for all protein-coding genes, ribosomal proteins (RP) and genes with high or low individual translation rates (TLRi; as described in Forés-Martos et al., 2021).

References

Amberg, D.C., Goldstein, A.L. & Cole, C.N. (1992). Isolation and characterization of RAT1: an essential gene of Saccharomyces cerevisiae required for the efficient nucleocytoplasmic trafficking of mRNA. Genes & Development, 6, 1173–1189.

Bashkirov, V.I., Solinger, J.A. & Heyer, W.D. (1995). Identification of functional domains in the Sep1 protein (= Kem1, Xrn1), which is required for transition through meiotic prophase in *Saccharomyces cerevisiae* . Chromosoma, 104 (3), 215-222. doi: 10.1007/BF00352186.

Basu, S., Mallik, S., Hait, S., & Kundu, S. (2021). Genome-scale molecular principles of mRNA half-life regulation in yeast. The FEBS Journal, 288 (11), 3428-3447. doi: 10.1111/febs.15670.

Benet, M., Miguel, A., Carrasco, F., Li, T., Planells, J., Alepuz, P., Tordera, V., & Pérez-Ortín, J.E. (2017). Modulation of protein synthesis and degradation maintains proteostasis during yeast growth at different temperatures. Biochimica et Biophysica Acta, Gene Regulatory Mechanisms, 1860 (7), 794-802. doi: 10.1016/j.bbagrm.2017.04.003.

Blasco-Moreno, B., de Campos-Mata, L., Böttcher, R., García-Martínez, J., Jungfleisch, J., Nedialkova, D.D., Chattopadhyay, S., Gas, M.E., Oliva, B., Pérez-Ortín, J.E., Leidel, S.A., Choder, M., & Díez, J. (2019). The exonuclease Xrn1 activates transcription and translation of mRNAs encoding membrane proteins. Nature Communications, 10 (1), 1298. doi: 10.1038/s41467-019-09199-6.

Braun, J.E., Truffault, V., Boland, A., Huntzinger, E., Chang, C.T., Haas, G., Weichenrieder, O., Coles, M., & Izaurralde, E. (2012). A direct interaction between DCP1 and XRN1 couples mRNA decapping to 5' exonucleolytic degradation. Nature Structural & Molecular Biology, 19 (12), 1324-1331. doi: 10.1038/nsmb.2413.

Chang, J.H., Xiang, S. & Tong, L. (2011). 50-30 Exoribonucleases. In: A. W. Nicholson (Ed.) Ribonucleases, Vol. 7. pp. 167–192, Heidelberg: Springer.

Chang, J.H., Xiang, S., & Tong, L. (2012). Structures of 5'-3' Exoribonucleases. Enzymes, 31, 15-29. doi: 10.1016/B978-0-12-404740-2.00006-9.

Chattopadhyay, S., García-Martínez, J., Haimovich, G., Fisher, J., Khwaja, A., Barkai, O.; Chuarzman, S.G., Schuldiner, M., Elran, R., Rosenberg, M., Urim, S., Desmukh, S., Bohnsack, K.E., Pérez-Ortín, J.E., & Choder, M. (2022). RNA-controlled nucleocytoplasmic shuttling of mRNA decay factors regulates mRNA synthesis and a mRNA decay pathway. Nature Communications, 13, 7184. doi: 10.1038/s41467-022-34417-z.

Choder, M. (2011). mRNA imprinting: Additional level in the regulation of gene expression. Cell Logistics, 1 (1), 37-40. doi: 10.4161/cl.1.1.14465.

Currie S.L., Xing W., Muhlrad D., Decker C.J., Parker R., Rosen M.K. (2020). Quantitative reconstitution of yeast RNA processing bodies. Proc Natl Acad Sci U S A. 120 (14), e2214064120. doi: 10.1073/pnas.2214064120.

Fares, M.A., Keane, O.M., Toft, C., Carretero-Paulet, L., & Jones, G.W. (2013). The roles of whole-genome and small-scale duplications in the functional specialization of *Saccharomyces cerevisiae* genes. PLoS Genetics, 9, e1003176.

Forés-Martos, J., Forte, A., García-Martínez, J., & Pérez-Ortín, J.E. (2021). A trans-omics comparison reveals common gene expression strategies in four model organisms and exposes similarities and differences between them. Cells, 10 (2), 334. doi: 10.3390/cells10020334.

García-Martínez, J., Aranda, A., & Pérez-Ortın, J.E. (2004). Genomic Run-On evaluates transcription rates for all yeast genes and identifies gene regulatory mechanisms. Molecular Cell, 15, 303–313.

García-Martínez, J., Delgado-Ramos, L., Ayala, G., Pelechano, V., Medina, D.A., Carrasco, F., González, R., Andrés-León, E., Steinmetz, L., Warringer, J., Chavez, S., & Pérez-Ortín, J.E. (2016). The cellular growth rate controls overall mRNA turnover, and modulates either transcription or degradation rates of particular gene regulons. Nucleic Acids Research, 44, 3643–3658.

Gietz, R.D. & Schiestl, R.H. (2007). High-efficiency yeast transformation using the LiAc/SS carrier DNA/PEG method. Nature Protocols, 2 (1), 31-34. doi: 10.1038/nprot.2007.13.

Haimovich, G., Medina, D.A., Causse, S.Z., Garber, M., Millán-Zambrano, G., Barkai, O., Chávez, S., Pérez-Ortín, J.E., Darzacq, X., & Choder, M. (2013). Gene expression is circular: factors for mRNA degradation also foster mRNA synthesis. Cell, 153 (5), 1000-1011. doi: 10.1016/j.cell.2013.05.012.

Han, W.Y., Hou, B.H., Lee, W.C., Chan, T.C., Lin, T.H., & Chen, H.M. (2023). Arabidopsis mRNA decay landscape shaped by XRN 5'-3' exoribonucleases. Plant Journal, 114, 895-913. doi: 10.1111/tpj.16181.

Heyer, W.D., Johnson, A.W., Reinhart, U. & Kolodner, R.D. (1995). Regulation and intracellular localization of Saccharomyces cerevisiae strand exchange protein 1 (Sep1/Xrn1/Kem1), a multifunctional exonuclease. Molecular and Cellular Biology, 15, 2728–2736.

Huch, S., Nersisyan, L., Ropat, M., Barret, D., Wu, M., Wang, J., Valeriano, V.D., Vardazaryan, N., Huertas-Cepas, J., Wei, W., Steinmetz, L., Engstrand, L., & Pelechano, V. (2023). Atlas of mRNA translation and decay for bacteria. Nature Microbiology, 8, 1123-1136. doi:10.1038/s41564-023-01393-z.

Ishikawa, M., Díez, J., Restrepo-Hartwig, M., & Ahlquist P. (1997). Yeast mutations in multiple complementation groups inhibit brome mosaic virus RNA replication and transcription and perturb regulated expression of the viral polymerase-like gene. Proceedings of the National Academy of Sciences USA, 94 (25), 13810-13815. doi: 10.1073/pnas.94.25.13810.

Johnson, A.W. (1997). Rat1p and Xrn1p are functionally interchangeable exoribonucleases that are restricted to and required in the nucleus and cytoplasm, respectively. Molecular and Cell Biology, 17 (10), 6122-6130.

doi: 10.1128/MCB.17.10.6122.

Johnson, A.W., & Kolodner, R.D. (1995). Synthetic lethality of sep1 (xrn1) ski2 and sep1 (xrn1) ski3 mutants of Saccharomyces cerevisiae is independent of killer virus and suggests a general role for these genes in translation control. Molecular and Cell Biology, 15 (5), 2719-2727. doi: 10.1128/MCB.15.5.2719.

Kenna, M., Stevens, A., McCammon, M., & Douglas, M.G. (1993). An essential yeast gene with homology to the exonuclease-encoding XRN1/KEM1 gene also encodes a protein with exoribonuclease activity. Molecular and Cell Biology, 13 (1), 341-350. doi: 10.1128/mcb.13.1.341-350.1993.

Kim, M., Krogan, N.J., Vasiljeva, L., Rando, O.J., Nedea, E., Greenblatt, J.F., and Buratowski,S. (2004). The yeast Rat1 exonuclease promotes transcription termination by RNA polymerase II. Nature, 432 (7016), 517-522. doi: 10.1038/nature03041.

Langeberg, C.J., Welch, W.R.W., McGuire, J.V., Ashby, A., Jackson, A.D., & Chapman, E.G. (2020). Biochemical Characterization of Yeast Xrn1. Biochemistry, 59, 1493-1507. doi: 10.1021/acs.biochem.9b01035.

Larimer, F.W., & Stevens, A. (1990). Disruption of the gene XRN1, coding for a 5'—-3' exoribonuclease, restricts yeast cell growth. Gene, 95 (1), 85-90. doi: 10.1016/0378-1119(90)90417-p.

Larimer, F.W., Hsu, C.L., Maupin, M.K., & Stevens A. (1992). Characterization of the XRN1 gene encoding a 5'–>3' exoribonuclease: sequence data and analysis of disparate protein and mRNA levels of gene-disrupted yeast cells. Gene, 120 (1), 51-57. doi: 10.1016/0378-1119(92)90008-d.

Medina, D.A., Jordán-Pla, A., Millán-Zambrano, G., Chávez, S., Choder, M., & Pérez-Ortín, J.E. (2014). Cytoplasmic 5'-3' exonuclease Xrn1p is also a genome-wide transcription factor in yeast. Frontiers in Genetics, 5, 1. doi: 10.3389/fgene.2014.00001.

Nagarajan, V.K., Jones, I., Newbury, S.F., & Green, P.J. (2013). XRN 5'-3' exoribonucleases: structure, mechanisms and functions. Biochimica et Biophysica Acta, Gene Regulatory Mechanisms, 1829, 590-603. doi: 10.1016/j.bbagrm.2013.03.005.

Nersisyan, L., Ropat, M., & Pelechano,V. (2020). Improved computational analysis of ribosome dynamics from 5'P degradome data using fivepseq. NAR Genomics and Bioinformatics, 2 (4), lqaa099. doi: 10.1093/nargab/lqaa099.

Oliete-Calvo, P., Serrano-Quilez, J., Nuno-Cabanes, C., Perez-Martinez, M.E., Soares, L.M., Dichtl,B ., Buratowski, S., Perez-Ortin, J.E., & Rodriguez-Navarro, S. (2018). A role for Mog1 in H2Bub1 and H3K4me3 regulation affecting RNAPII transcription and mRNA export. EMBO Reports, 19 (11), e45992. doi: 10.15252/embr.201845992.

Page, A.M., Davis, K., Molineux, C., Kolodner, R.D., & Johnson, A.W. (1998). Mutational analysis of exoribonuclease I from*Saccharomyces cerevisiae* . Nucleic Acids Research, 26 (16), 3707-3716. doi: 10.1093/nar/26.16.3707.

Parker, R., & Song, H. (2004). The enzymes and control of eukaryotic mRNA turnover. Nature Structural and Molecular Biology, 11 (2), 121-127. doi: 10.1038/nsmb724.

Parker, R. (2012). RNA degradation in *Saccharomyces cerevisiae* . Genetics, 191 (3), 671-702. doi: 10.1534/genetics.111.137265.

Pelechano, V., & Perez-Ortin, J.E. (2008). The transcriptional inhibitor thiolutin blocks mRNA degradation in yeast. Yeast, 25 (2), 85-92. doi: 10.1002/yea.1548.

Pelechano, V., Wei, W., & Steinmetz, L.M. (2015). Widespread co-translational RNA decay reveals ribosome dynamics. Cell, 161, 1400–1412.

Pelechano, V., Wei, W., & Steinmetz, L.M. (2016). Genome-wide quantification of 5'P-phosphorylated mRNA degradation intermediates for analysis of ribosome dynamics. Nature Protocols, 11, 359–376.

Perez-Ortin, J.E., & Chavez, S. (2022). Nucleo-cytoplasmic shuttling of RNA-binding factors: mRNA buffering and beyond. Biochimica et Biophysica Acta, Gene Regulatory Mechanisms, 1865, (5), 194849. doi: 10.1016/j.bbagrm.2022.194849.

Ramırez, F., Ryan, D.P., Grüning, B., Bhardwaj, V., Kilpert, F., Richter, A.S., Heyne, S., Dündar, F., & Manke, T. (2016). deepTools2: a next generation web server for deep-sequencing data analysis. Nucleic Acids Research, 44 (W1), W160–W165. doi: 10.1093/nar/gkw25.

Sharma, S., Yang, J., Grudzien-Nogalska, E., Shivas, J., Kwan, K.Y., & Kiledjian, M. (2022). Xrn1 is a deNADding enzyme modulating mitochondrial NAD-capped RNA. Nature Communications, 13 (1), 889. doi: 10.1038/s41467-022-28555-7.

Shen, L., Shao, N., Liu, X., &Nestler, E. (2014). ngs.plot: Quick mining and visualization of next-generation sequencing data by integrating genomic databases. BMC Genomics, 15, 284. doi: 10.1186/1471-2164-15-284.

Sun, M., Schwalb, B., Pirkl, N., Maier, K.C., Schenk, A., Failmezger, H., Tresch, A., & Cramer, P. (2013). Global analysis of eukaryotic mRNA degradation reveals Xrn1-dependent buffering of transcript levels. Molecular Cell, 52, 52–62.

Tesina, P., Heckel, E., Cheng, J., Fromont-Racine, M., Buschauer, R., Kater, L., Beatrix, B., Berninghausen, O., Jacquier, A., Becker, T., & Beckmann, R. (2019). Structure of the 80S ribosome-Xrn1 nuclease complex. Nature Structural & Molecular Biology, 26 (4), 275-280. doi: 10.1038/s41594-019-0202-5.

Wolfe, K.H. (2015). Origin of the yeast whole-genome duplication. PLoS Biology, 13 (8), e1002221. doi: 10.1371/journal.pbio.1002221.

Xu, Z., Wei, W., Gagneur, J., Perocchi, F., Clauder-Münster, S., Camblong, J., Guffanti, E., Stutz, F., Huber, W., & Steinmetz, L.M. (2009). Bidirectional promoters generate pervasive transcription in yeast. Nature, 457 (7232), 1033-1037. doi: 10.1038/nature07728.

Zhang, Y., & Pelechano, V. (2021). Application of high-throughput 5'P sequencing for the study of co-translational mRNA decay. STAR Protocols, 2 (2), 100447. doi: 10.1016/j.xpro.2021.100447.

Figure 1

A

Strain	Relative generation time	Relative cell volume	Relative global poly(A) half-life	Relative global [mRNA]
wt + YCpLac33	1.00	1.00	1.00	1.00
wt + pBBM3 (cRat1)	1.06 ± 0.06	0.96 ± 0.06	0.98 ± 0.17	1.36
xrn1Δ + YCpLac33	1.44 ± 0.06	1.53 ± 0.05	2.43 ± 0.84	0.84
xrn1Δ + pBBM3 (cRat1)	1.22 ± 0.01	1.07 ± 0.04	1.38 ± 0.14	0.74

B

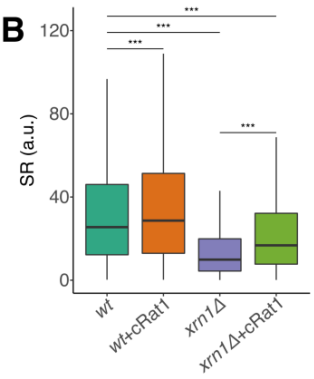

Figure 2